scientific reports

Check for updates

OPEN

Airway ciliary microenvironment responses in mice with primary ciliary dyskinesia and central pair apparatus defects

Casey W. McKenzie[1], Reesa M. Wilcox[1], Oduduabasi J. Isaiah[2], Michael S. Kareta[3,4] & Lance Lee[1,4]✉

Dysfunction of motile cilia can impair mucociliary clearance in the airway and result in primary ciliary dyskinesia (PCD). We previously showed that mutations in central pair apparatus (CPA) genes perturb ciliary motility and result in PCD in mouse models. However, little is known about how epithelial cell types in the ciliary microenvironment of the upper airway respond to defects in ciliary motility and mucociliary clearance. Here, we have used single-cell RNA sequencing to investigate responses in tracheal epithelial cells from mice with mutations in CPA genes *Cfap221/Pcdp1*, *Cfap54*, and *Spef2*. Expected cell types were identified, along with an unidentified cell type not expressing markers of typical airway cells. Deuterosomal cells were found to exist in two states that differ largely in expression of genes involved in differentiation into ciliated cells. Functional enrichment analysis of differentially expressed genes (DEGs) revealed important cellular functions and molecular pathways for each cell type that are altered in mutant mice. Overlapping DEGs shed light on general responses to cilia dysfunction, while unique DEGs indicate that some responses may be specific to the individual mutation and ciliary defect.

Keywords Motile cilia, Primary ciliary dyskinesia, Central pair, Airway, Single cell RNAseq

Defects in motile cilia typically result in the pediatric syndrome primary ciliary dyskinesia (PCD) due to an inability of the cilia to clear fluids and particles from the epithelial cell surface[1–3]. Mucociliary clearance defects in the airway cause patients to experience chronic upper and lower respiratory infections, bronchiectasis, and a decline in pulmonary function[1–3]. Similarly, dysfunction of ependymal cilia in the brain and epithelial cilia in the oviduct can result in hydrocephalus and female infertility, respectively, in some patients[1–3]. Situs inversus is also associated with PCD due to defects in the similarly structured nodal cilia during embryonic development, and defects in sperm flagella commonly cause male infertility[1–3]. PCD is a genetically heterogeneous disorder[1–3], and while there has been a substantial body of research investigating the impact of gene mutations on ciliary function, little is known about how the cells in the ciliary microenvironment, or the airway epithelial milieu, respond to cilia dysfunction during disease pathogenesis.

In the airway, the ciliary microenvironment consists of several epithelial cell types (Fig. 1A)[4]. The primary differentiation pathway involves basal progenitor cells differentiating into suprabasal cells, which further differentiate into secretory club cells (also known as Clara cells). In the presence of Notch signaling, club cells can differentiate into mucus-producing Goblet cells. In the absence of Notch, both club and goblet cells give rise to deuterosomal cells, which further differentiate into ciliated cells. Several rare cell types are also found in the airway, including tuft cells, ionocytes, and neuroendocrine cells. While each cell type has distinct and critical functions within the airway, it remains unclear how each responds to defects in mucociliary clearance, the primary function of ciliated cells, to address this physiological abnormality. Moreover, it is unclear how mutations in different ciliary genes affect disease pathogenesis at the cellular level in the airway.

Recent single-cell transcriptomic studies using human tissue, mouse models, and cultured epithelial cell systems have shed light on the composition of the mammalian airway epithelium[4–7]. This studies have identified

[1]Pediatrics and Rare Diseases Group, Sanford Research, 2301 E. 60th St. N., Sioux Falls, Sioux Falls, SD 57104, USA. [2]Functional Genomics and Bioinformatics Core, Sanford Research, 2301 E. 60th St. N., Sioux Falls, SD 57104, USA. [3]Genetics and Genomics Group, Sanford Research, 2301 E. 60th St. N., Sioux Falls, SD 57104, USA. [4]Department of Pediatrics, Sanford School of Medicine of the University of South Dakota, 1400 W. 22nd Street, Sioux Falls, SD 57105, USA. ✉email: lance.lee@sanfordhealth.org

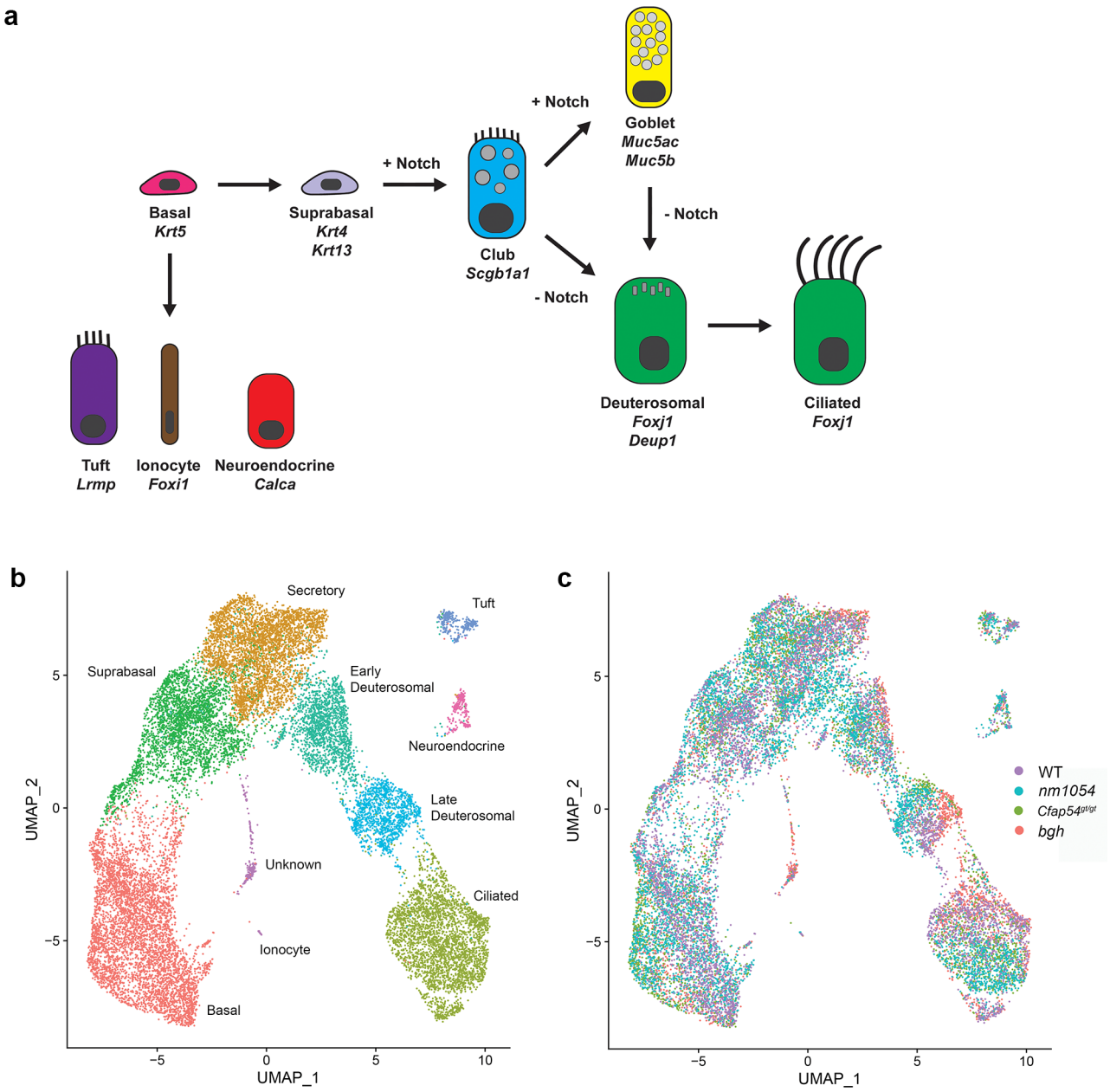

Fig. 1. Expected cell types identified in PCD mouse tracheae. (**A**) Schematic diagram depicting the current understanding of cellular differentiation in the upper airway. Cell-specific markers used to identify the cell types are provided in italics. (**B**-**C**) UMAP plots showing individual cell clusters in the mouse tracheal epithelium, depicted as combined for all genotypes (**B**) and separated by genotype (**C**). Each dot represents an individual cell plotted by gene expression profile.

several critical cell types and their differentiation pathways[4–7]. Transcriptomic studies have also demonstrated that the major airway cell types are heterogeneous populations with differences between the upper and lower airway, as well as between the fetal and adult airways[6,8–14]. In addition, recent work has demonstrated that motile ciliated cells in the airway and other tissues share cilia-related gene expression profiles and undergo a convergent differentiation pathway[15].

Transcriptomic studies have also begun to identify differences between wild type (WT) cells and airway epithelial cells in disease states. Reyfman et al. compared human lung tissue between healthy transplant donors and transplant recipients with pulmonary fibrosis, identifying changes in gene expression in multiple cell types in the fibrotic lungs and uncovering novel sub-populations of alveolar epithelial cells and alveolar macrophages in the lower airway of patients with pulmonary fibrosis[16]. Biopsies from cystic fibrosis (CF) patients with end-stage lung disease identified substantial changes in gene expression in each of the major epithelial cell types compared to healthy patients[17]. Sorted basal cells from COPD patients similarly showed substantial differences in gene

expression profiles[10]. Only a couple of studies have begun to apply single cell transcriptomic approaches to the PCD airway. Yang et al. identified basal, cycling basal, suprabasal, club, goblet, and ciliated cells in organoids cultured from a tracheobronchial biopsy from a PCD patient with a mutation in the dynein gene *DNAH5*[18]. Horani et al. identified basal cells, secretory cells, ciliated cells, ionocytes, and neuroendocrine cells in tracheal epithelial cell cultures from a mouse model lacking dynein assembly factor Dnaaf5[19]. They demonstrated that while there was no apparent effect on distribution of cell types in the mutant culture, there was an increase in expression of cilia assembly and cilia component genes. Additional studies are required to fully understand the effects of cilia dysfunction on the ciliary microenvironment in vivo and understand how ciliary defects impact cellular functions during disease pathogenesis.

We previously showed that mutations in ciliary central pair apparatus (CPA) genes *Cfap221* (also known as *Pcdp1*), *Cfap54*, and *Spef2* result in a PCD phenotype due to defects in ciliary motility[20–22]. The mutant airways exhibit mucociliary clearance defects with an accumulation of mucus in the maxillary sinus cavity that is sometimes accompanied by an immune response. In addition, exposure to the bacterium *Streptococcus pneumoniae*, a common pathogen in PCD patients, results in an enhanced immune response in mice with mutations in *Cfap221* or *Spef2*[23]. Importantly, mutations in *CFAP221*, *SPEF2*, and *CFAP54* have since been identified in human PCD patients[24–26], underscoring the significance of these genes in ciliary function and human health. We hypothesized that airway epithelial cells undergo specific cellular responses to ciliary dysfunction during disease pathogenesis. In this study, we have used a scRNAseq approach to understand how the epithelial cell types in the airway ciliary microenvironment respond to defects in cilia function in these three models of PCD. The use of three different CPA models strengthens the findings and provides evidence for cellular mechanisms altered under conditions of impaired mucociliary clearance, while simultaneously uncovering differences due to mutations in distinct CPA genes. We report changes in gene expression profiles in each of the primary epithelial cell types (basal, suprabasal, secretory, deuterosomal, and ciliated) from each mutant mouse line. We also identify functional categories and affected molecular pathways for differentially expressed genes that indicate cellular responses to ciliary dysfunction. In addition, we provide evidence that deuterosomal cells may exist as two distinct cell types that vary in their state of differentiation toward ciliated cells. While previous studies have used cultured human or mouse airway epithelial cells, to our knowledge, this is the first study to use a single-cell transcriptomic approach to investigate cellular responses to motile cilia dysfunction in vivo.

Results

Single-cell RNAseq analysis reveals expected airway cell types in tracheae with CPA defects

To elucidate how epithelial cells in the airway respond to defects in ciliary motility and mucociliary clearance, we performed a scRNAseq analysis on the tracheal epithelium from three mouse models with CPA defects whose phenotypes we had previously characterized in detail[20–23], and we compared those to WT mice. Figure 1A shows the cell types within the upper airway epithelium and their differentiation pathway. Through single cell sorting, we obtained transcript sequence for all expected cell types as determined by marker expression analysis, as well as an additional unidentified cell cluster (Fig. 1B). All cell types were present in WT and each PCD mutant mouse (Fig. 1C).

Cell clusters were defined by identifying cell-specific marker expression using the 10X Genomics Loupe browser software (Fig. 2). Basal cells were defined by expression of *Krt5* and *Tp63* (Fig. 2). Similarly, *Itga6* and *Ghrl2* are both markers of undifferentiated cells. *Ghrl2* did not appear at substantial levels in any tracheal epithelial cluster, but *Itga6* was expressed in all clusters except the most terminally differentiated, which we determined to be the ciliated cells (Fig. 2). *Krt4* and *Krt13* are markers of suprabasal cells, with *Krt4* expressed in a larger cluster of cells (Fig. 2). Secretory cells were generally identified by expression of *Bpifa1* and *Wfdc2*. These markers are expressed in multiple clusters, including clusters that overlap with suprabasal cell marker *Krt4* and clusters that overlap with deuterosomal marker *Deup1* (Fig. 2). We therefore conclude that the suprabasal cells, which give rise to secretory cells, are beginning to express secretory cell genes. Similarly, deuterosomal cells, which differentiate from secretory cells, are still expressing some secretory cell genes. The cluster between those, which only expresses secretory cell markers, likely represents the secretory cells. To distinguish between secretory cell types, we examined expression of club cell marker *Scgb1a1* and goblet cell marker *Muc5b*. These markers are expressed in overlapping clusters (Fig. 2), suggesting that the two secretory cell types have very similar gene expression profiles and are both represented by the same secretory cell cluster. Deuterosomal cells were identified by *Deup1* and *Plk4*, which appear in two distinct clusters based on overall gene expression profile in the UMAP plot (Fig. 2). *Foxj1* and *Tub1a1* are expressed in both deuterosomal and ciliated cells. These markers identify the two deuterosomal clusters and an additional cluster that we determined to be the ciliated cells (Fig. 2). The absence of *Itga6*, a marker of undifferentiated cells, in that third cluster provides additional evidence that this cluster represents the terminally differentiated ciliated cells. The deuterosomal and ciliated cell clusters were further defined by expression of *eGFP*, which is expressed as a transgene under the *Foxj1* promoter in our mouse lines as a control for the scRNAseq approach and identifies ciliated and deuterosomal cells, as well as cilia genes *Dnah5* and *Dnah12* (Fig. S1). We also verified that the genes mutated in each mouse line (*Cfap221* in the *nm1054* mouse, *Cfap54* in the *Cfap54*$^{gt/gt}$ mouse, and *Spef2* in the *bgh* mouse) are expressed in the deuterosomal and ciliated cell clusters (Fig. S1). Cell clusters corresponding to the rarer tuft and neuroendocrine cell types were identified by *Lrmp* and *Calca*, respectively (Fig. 2). Ionocyte marker *Foxi1* identified only a very small cell cluster (Fig. 2). *Cftr*, which is expressed at low level in most airway epithelial cell types, is known to be expressed at highest levels in ionocytes[5,6], and its highest expression level is in the same *Foxi1*-positive cluster that we deem to represent ionocytes (Fig. 2). *Ccna* and *Hells* were used as markers of rapidly dividing cells, since the tuft cells, ionocytes, and neuroendocrine cells were previously found to rapidly derive from the basal cells (Montoro 2018). Surprisingly, these markers were found only in a small subset of cells between the secretory and

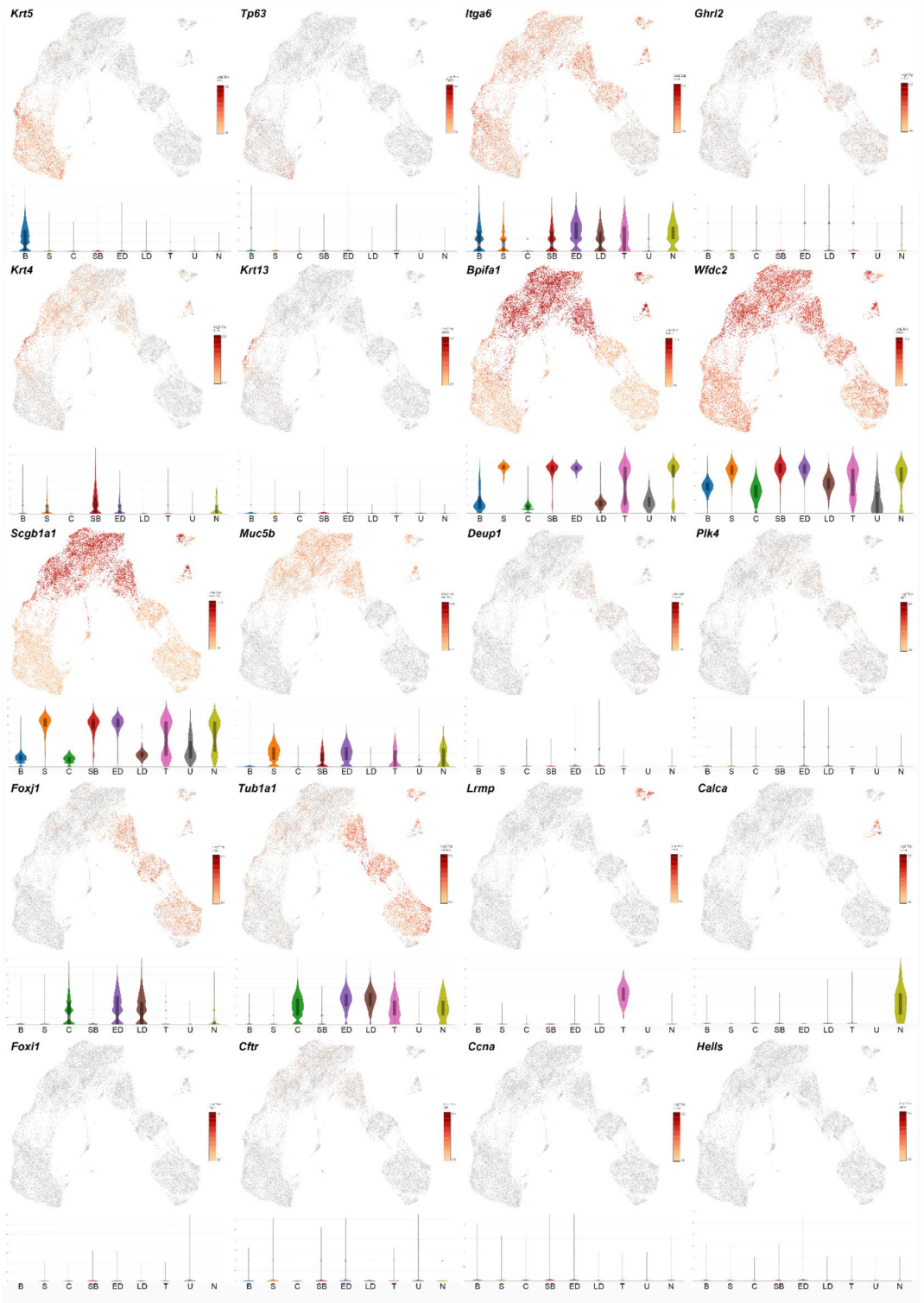

Fig. 2. Expression of cell-specific markers in the mouse tracheal epithelium. UMAP plots and violin plots showing marker expression by cell type are provided for *Krt5* (basal), *Tp63* (basal), *Itga6* (non-terminally differentiated cells), *Ghrl2* (undifferentiated cells), *Krt4* (suprabasal), *Krt13* (suprabasal), *Bpifa1* (secretory), *Wfdc2* (secretory), *Scgb1a1* (Club cells), *Muc5b* (Goblet cells), *Deup1* (deuterosomal), *Plk4* (deuterosomal), *Foxj1* (deuterosomal and ciliated), *Tub1a1* (deuterosomal and ciliated), *Lrmp* (tuft), *Calca* (neuroendocrine), *Foxi1* (ionocyte), *Cftr* (ionocyte), *Ccna* (rapidly dividing cells), and *Hells* (rapidly dividing cells). B: basal cells, C: ciliated cells, ED: early deuterosomal cells, LD: late deuterosomal cells, N: neuroendocrine cells, S: secretory cells, SB: suprabasal cells, T: tuft cells, U: unknown cell cluster.

deuterosomal cells, rather than in the expected basal cells (Fig. 2). Combined, marker expression demonstrates effective identification of known epithelial cell types in the airway.

One cell cluster, labeled as Unknown in Fig. 1B, was negative for all markers of expected tracheal epithelial cell types. To determine if it might be a contaminating cell type in our prep, we investigated whether it expresses markers of common airway contaminants. We first investigated whether it might be cluster of cells undergoing apoptosis that have a distinct expression profile. Apoptosis scoring showed positively apoptotic cells in nearly every cluster, but the Unknown cluster was not uniquely higher than any other (Fig. S2). Similarly, apoptotic marker *Bcl2* did not show high expression in the Unknown cluster (Fig. S2). *Vim* is a marker of fibroblasts, which are separated away from the epithelial cells prior to single-cell sorting. To determine whether a cluster of fibroblasts may have remained with the cell prep, we examined *Vim* expression but found only negligible levels of expression throughout the various clusters with no increase in the Unknown cluster (Fig. S2), suggesting that the protocol was effective at removing fibroblasts from the sample. In addition, no expression of airway smooth muscle marker *Myh11* was detected in the Unknown cluster (Fig. S2). Also not expressed in that cluster was hematopoietic marker *Ptprc* (Fig. S2), indicating that there are no contaminating red or white blood cells in the sample. Finally, we examined markers of immune cells that might infiltrate the upper airway. No marked expression of macrophage marker *CD68*, T lymphocyte marker *CD3D*, or B lymphocyte marker *CD19* was observed in the Unknown cluster (Fig. S2). Given the common origin of the airway and intestine from the developing gut tube, along with the presence of tuft cells and ionocytes in both systems, we investigated whether the Unknown cluster could represent an intestinal cell type not previously appreciated in the airway. We examined markers for crypt cells (*Lgr5*), Paneth cells (*Lyz1*), M cells (*Tnfaip2*), faveolar cells (*Aplnr*), parietal cells (*Atp4a*), and enterochromaffin cells (*Spock1*). However, no discernable expression was observed for any of these markers in our cell samples (Fig. S3). We then compared the gene expression profile for the WT Unknown cell cluster to all other clusters in the WT sample in an effort to identify potential cellular functions that are unique to that cell type (Table S1). Gene ontology (GO) enrichment analysis identified the top functional categories as myelin sheath, endoplasmic reticulum (ER), and cytosolic small ribosomal subunit (Fig. S4). Processes related to the ER or translation do not provide any substantial information regarding the function of this cell type. The myelin sheath is specific to neurons, so while a nervous system origin could be of potential relevance, additional studies are required to further elucidate the identity of this cell cluster.

To further investigate the relationship between the cell clusters, we performed pseudotime analysis using both the Monocle (Fig. 3A) and Slingshot (Fig. 3B-C) software. Differentiation of epithelial cells begins with the basal cell cluster. As expected, the primary differentiation pathway leads through the suprabasal cells, secretory cells, deuterosomal cells, and concludes with the terminally differentiated ciliated cells. Surprisingly, the pseudotime analysis suggests that the neuroendocrine cells and tuft cells may derive from the deuterosomal cells in a separate lineage from the ciliated cells. This is supported by expression of secretory cell markers (*Bpifa1*, *Wfdc2*, *Scgb1a1*, *Muc5b*) and deuterosomal/ciliated cell markers (*Foxj1*, *Tub1a1*) in the neuroendocrine and tuft cell clusters (Fig. 2). Pseudotime analysis also suggests that the differentiating suprabasal cells may give rise to the Unknown cell cluster and the ionocytes in an additional lineage (Fig. 3). While further experimental evidence is needed to fully discern the differentiation pathways for these cells, the pseudotime analysis confirms the primary differentiation pathway to the ciliated cells and suggests a more complicated pathway for differentiation of rare epithelial cell types.

Deuterosomal cells appear in two distinct clusters

Pseudotime analysis suggests that the two deuterosomal cell clusters exist as early and late deuterosomal cells along the primary differentiation pathway to ciliated cells (Fig. 3). To further discern the relationship between

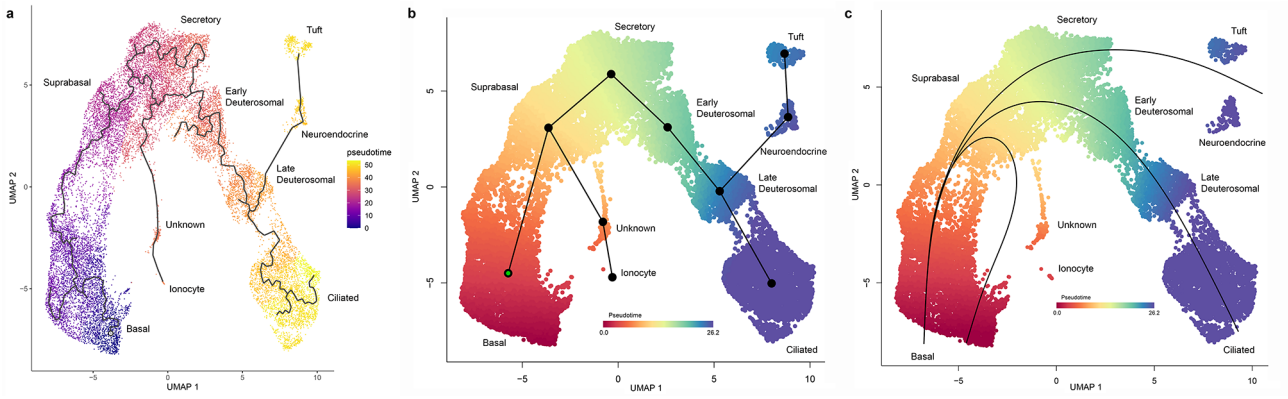

Fig. 3. Pseudotime analysis of cell types in PCD mouse tracheae. UMAP plots generated through Monocle (**A**) and Slingshot (**B**, **C**) software showing that cells likely follow a differentiation path from basal to suprabasal, secretory, early deuterosomal, late deuterosomal, and finally ciliated cells as a terminally differentiated cell type. The plots show trajectories (**A**, **B**) and lineages (**C**). The plots also raise the possibility that neuroendocrine and tuft cells may differentiate from deuterosomal cells in a distinct lineage and that the unknown cell cluster and ionocytes may differentiate directly from secretory cells in a separate lineage.

these two deuterosomal cell clusters, we used GO enrichment analysis to compare the gene expression profiles between the two clusters from WT tracheae (Fig. 4A, Table S2). The top functional categories fell into three main areas: microtubule cytoskeleton (microtubule-based process, microtubule-based movement, cytoskeleton, microtubule cytoskeleton), cell projection (plasma membrane bounded cell projection assembly, cell projection assembly), and ciliogenesis (cilium assembly, cilium organization, motile cilium). Since cilia are microtubule-based organelles that extend from the cell surface, these top functional categories all point to differences related to differentiation into the ciliated cell type. Pathway analysis identified several relevant pathways that were altered in the late deuterosomal cells relative to the early deuterosomal cells. Notably, a large number of genes in the cilium assembly pathway are up-regulated in late deuterosomal cells (Fig. 4B). In addition, there is down-regulation of key components of the gap junction signaling pathway along with up-regulation of components of tight junction signaling and epithelial adherens junction signaling that are predicted to lead to enhanced cytoskeletal rearrangement and cell differentiation (Fig. 4C-E). Interestingly, there is also an up-regulation of genes involved in the Wnt signaling pathway (Fig. 4F), which has been shown to play an important role in driving motile ciliogenesis[27,28]. We therefore conclude that the identified clusters of early deuterosomal cells

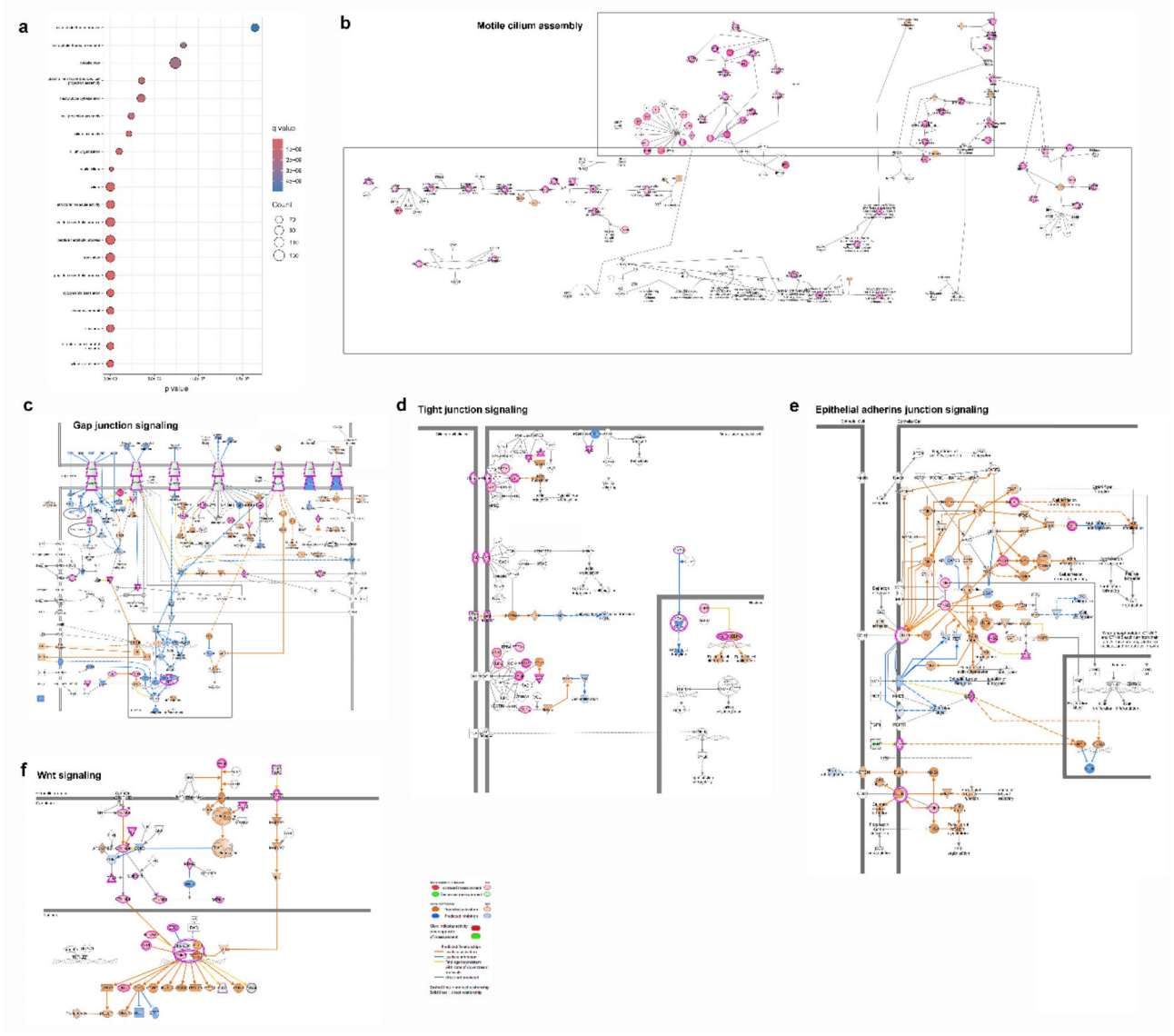

Fig. 4. Early and late deuterosomal cells are at distinct differentiation stages toward the ciliated cell type. (**A**) Bubble plot showing the top functional categories for genes differentially expressed between the WT early deuterosomal and late deuterosomal cell clusters indicate. The top functional categories pertain to microtubule processes, plasma membrane projection, and ciliogenesis. Functional categories were determined by GO analysis. (**B**-**F**) Altered molecular pathways in the late deuterosomal cells relative to the early deuterosomal cells showing differences in the motile cilia assembly (**B**), gap junction signaling (**C**), tight junction signaling (**D**), epithelial adherins junction signaling (**E**), and Wnt signaling (**F**) pathways. Pathways were generated using the Qiagen Ingenuity Pathway Analysis software.

and late deuterosomal cells exist at different but distinct stages of differentiation toward the ciliated cell type, with distinct changes in ciliogenesis, cell surface components, and cell-cell contact that may be driven by Wnt signaling.

Airway epithelial cell types show different expression profiles in mice with ciliary CPA defects

Differential gene expression (DEG) analysis was used to identify cellular responses to defects in ciliary motility and mucociliary clearance in the ciliary microenvironment. Genotyping and next-generation sequencing confirmed the presence of the underlying mutations in *nm1054*, *bgh*, and *Cfap54*$^{gt/gt}$ mice[20–22], and UMAP plots show the cluster-specific similarity between cells from WT, *nm1054*, *bgh*, and *Cfap54*$^{gt/gt}$ mice (Fig. 5). While there are basal, suprabasal, secretory, and early deuterosomal cells with distinct gene expression profiles for each genotype, separation of genotypes based on gene expression becomes highly apparent for late deuterosomal and ciliated cells. The clear differences in gene expression profiles for late deuterosomal and ciliated cells from each genotype suggest that cellular responses to ciliary dysfunction may become more pronounced further into the differentiation pathway. These results also indicate that causative mutations in individual genes encoding CPA components can have profoundly differential effects on gene expression and cellular responses.

Since none of the primary clusters show completely overlapping gene expression profiles for the four genotypes, we further investigated the DEGs for each cell type. We examined differences in gene expression profile, functional categories represented by the DEGs, and the most significantly up-regulated and down-regulated genes for basal cells (Fig. S5, Table S3), suprabasal cells (Fig. S6, Table S4), secretory cells (Fig. S7, Table S5), early deuterosomal cells (Fig. S8, Table S6), late deuterosomal cells (Fig. S9, Table S7), and ciliated cells (Fig. S10, Table S8). Heat maps demonstrate substantial differences in the gene expression profiles for each cell type in the WT, *nm1054*, *bgh*, and *Cfap54*$^{gt/gt}$ tracheae. The number of DEGs for each cell type, as well as the number of overlapping genes that are differentially expressed in all three of the mutant tracheae, are shown in Table 1. There are a number of overlapping DEGs for each cell type, indicating that there are some cellular responses common to airway epithelial cells regardless of ciliary defect. At the same time, however, there is also a substantial number of unique DEGs, suggesting that the specific ciliary defect may determine some of the cellular responses, even when each mutation is in a CPA gene. GO enrichment analysis identified the top functional categories of DEGs

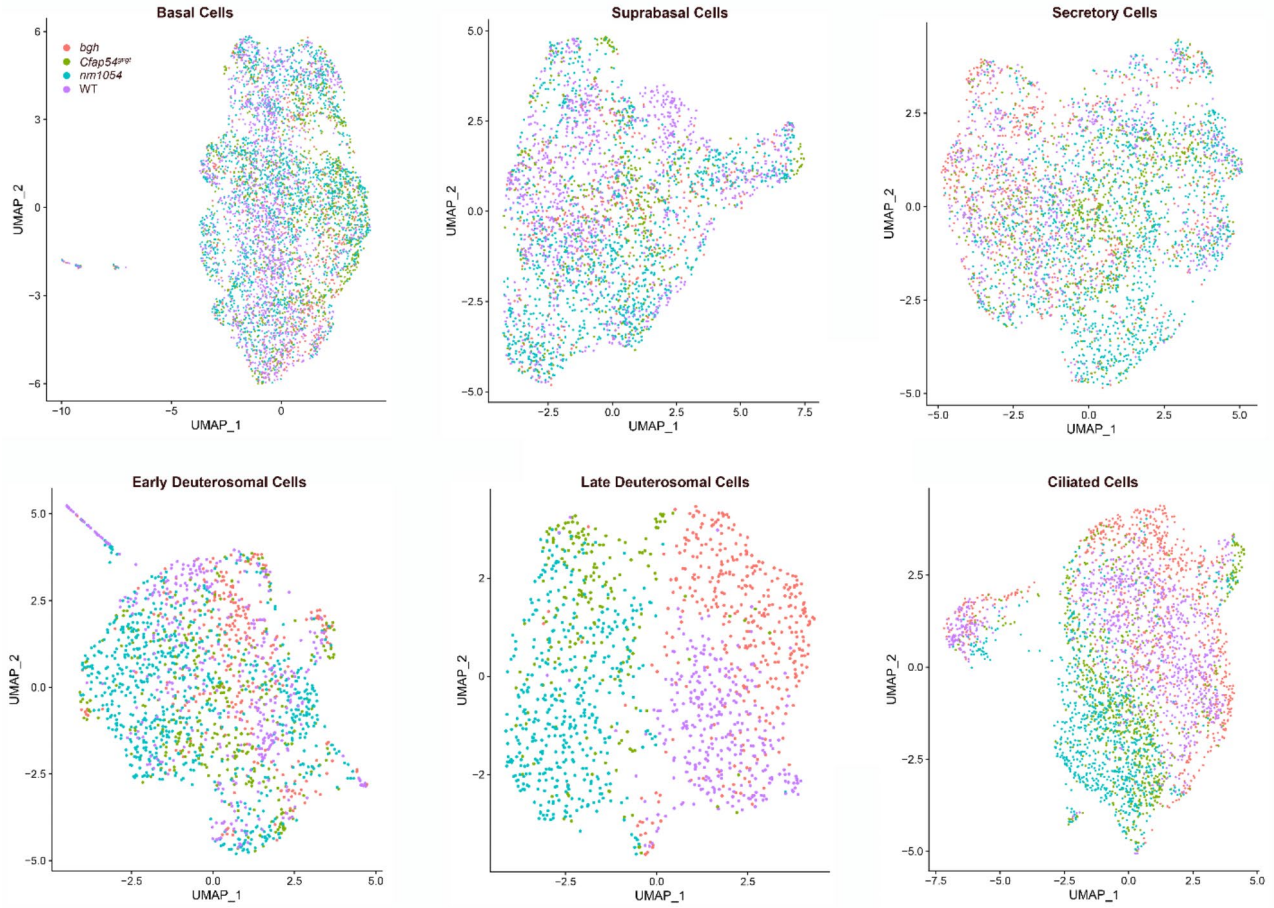

Fig. 5. Differences in gene expression profiles in PCD cell types. Cell cluster-specific UMAP plots separated by genotype for the primary epithelial cell types (basal, suprabasal, secretory, early deuterosomal, late deuterosomal, and ciliated). Each dot represents an individual cell plotted by gene expression profile.

Cell Type	DEGs in nm1054	DEGs in bgh	DEGs in Cfap54$^{gt/gt}$	Overlapping DEGs in all three mutants
Basal	220	312	361	69
Suprabasal	326	254	403	99
Secretory	204	244	324	78
Early Deuterosomal	306	454	653	102
Late Deuterosomal	503	527	649	79
Ciliated	144	144	140	24

Table 1. Numbers of differentially expressed genes (DEGs) in PCD epithelial cells.

for each epithelial cell type. While some functional categories were common across epithelial cell types, some functions particularly relevant to a given cell type emerged as responses to ciliary dysfunction. Finally, volcano plots indicate the most significantly up-regulated and down-regulated genes in each *nm1054*, *bgh*, and *Cfap54*$^{gt/gt}$ epithelial cell type. Because ribosomal genes were among the most significant DEGs in every cell type and for every genotype, we concluded that these genes are not directly relevant to the biological phenotype, and they were removed from all volcano plots in this study. Importantly, because the markers for club cells and goblet cells are expressed in an overlapping cluster (Fig. 2), DEGs were analyzed for the single secretory cell cluster without distinguishing between the two secretory cell types (Fig. S7). These results further underscore the differential impact of distinct PCD genotypes on gene expression and cellular function.

Key cellular functions and pathways are altered in mutant airway epithelial cells

Upon identification of top DEG functional categories for each epithelial cell type in our PCD mutant tracheae, we performed pathway analysis on a subset of high-interest functional categories that were prioritized based on their relevance to the airway phenotype. Notably, network diagrams show the relationship between DEGs involved in epithelial cell differentiation, an important altered pathway in basal cells from the PCD tracheae, suggesting that defects in mucociliary clearance may impact subsequent differentiation of epithelial cell types in the airway (Fig. 6A). Also highly relevant to cell differentiation in the airway, DEGs involved in the functional category of ciliogenesis and cilia function emerged in the late deuterosomal cells from *nm1054* and *Cfap54*$^{gt/gt}$ mice (Fig. 6B). Interestingly, an important functional category of DEGs identified for ciliated cells was immune response, particularly proteins with anti-bacterial function (Fig. 6C). With defects in ciliary function as the first means of host defense, it seems reasonable that ciliated cells would respond by activating mechanisms underlying an immune response as the next means of defense. Consistent with this finding, an infiltration of neutrophils was observed in the sinus cavity of *bgh* mice, as well as *bgh* double mutants with either the *nm1054* or the *Cfap54*$^{gt/gt}$ mutation[21,29].

In addition to functional categories for DEGs, we investigated impacts on individual molecular pathways relevant to the high-interest cellular functions. Interestingly, we observed down-regulation of several genes in the cilium assembly pathway in the late deuterosomal cells from all three PCD mutants (Fig. 7). Although we initially hypothesized that ciliary dysfunction might result in increased differentiation of ciliated cells to compensate for the defect, it appears as though the late deuterosomal cells may actually respond by reducing the number of new, defective ciliated cells. Given that inhibition of Notch signaling is a key driver of ciliated cell differentiation, we wondered whether Notch signaling would be affected in the PCD mutant cells. We observed changes in Notch signaling components only in the ciliated cells of the *Cfap54*$^{gt/gt}$ mutant, but there was an increase in the ubiquitinated form of the Notch signals and down-regulation of downstream components (Fig. S11), suggesting that there is further inactivation of Notch signaling. This indicates that the inhibition of ciliogenesis may be independent of Notch inactivation in the *Cfap54*$^{gt/gt}$ mutant. Finally, we observed increased expression in several major components of tight junction signaling in the secretory cells and early deuterosomal cells of *bgh* and *Cfap54*$^{gt/gt}$ mutant mice (Fig. S12), suggesting that mucociliary clearance defects may prompt cell surface and cell-cell contact changes at these key stages of epithelial differentiation, particularly in the absence of Spef2 or Cfap54. Taken together, these data demonstrate that epithelial cell types in the airway exhibit a variety of important responses to defects in ciliary motility during disease pathogenesis.

Discussion

In this study, we have performed the first in vivo scRNAseq analysis of epithelial cell types in the airway ciliary microenvironment from mice with primary defects in motile cilia function. Use of three mouse models with CPA defects lends strength to analysis of cellular responses to ciliary dysfunction and impaired mucociliary clearance while also highlighting differences in response based on the underlying PCD-causing mutation. Each of the expected epithelial cell types was identified in our samples, along with an Unknown cell cluster. Pseudotime analysis confirms the primary differentiation pathway toward the ciliated cell type and suggests a more complicated pathway for differentiation of rare epithelial cell types. The deuterosomal cells were found to exist in two distinct clusters that differ in their state of differentiation toward ciliated cells. Gene expression profile differences for each cell type uncovered distinct differences in cellular responses for each PCD model, indicating that the individual mutated CPA gene has a profound impact on cellular responses in the airway during disease pathogenesis. Functional enrichment analysis of the differentially expressed genes uncovered a variety of cellular functions altered in mutant cells, including those required for differentiation, ciliogenesis, and immune response.

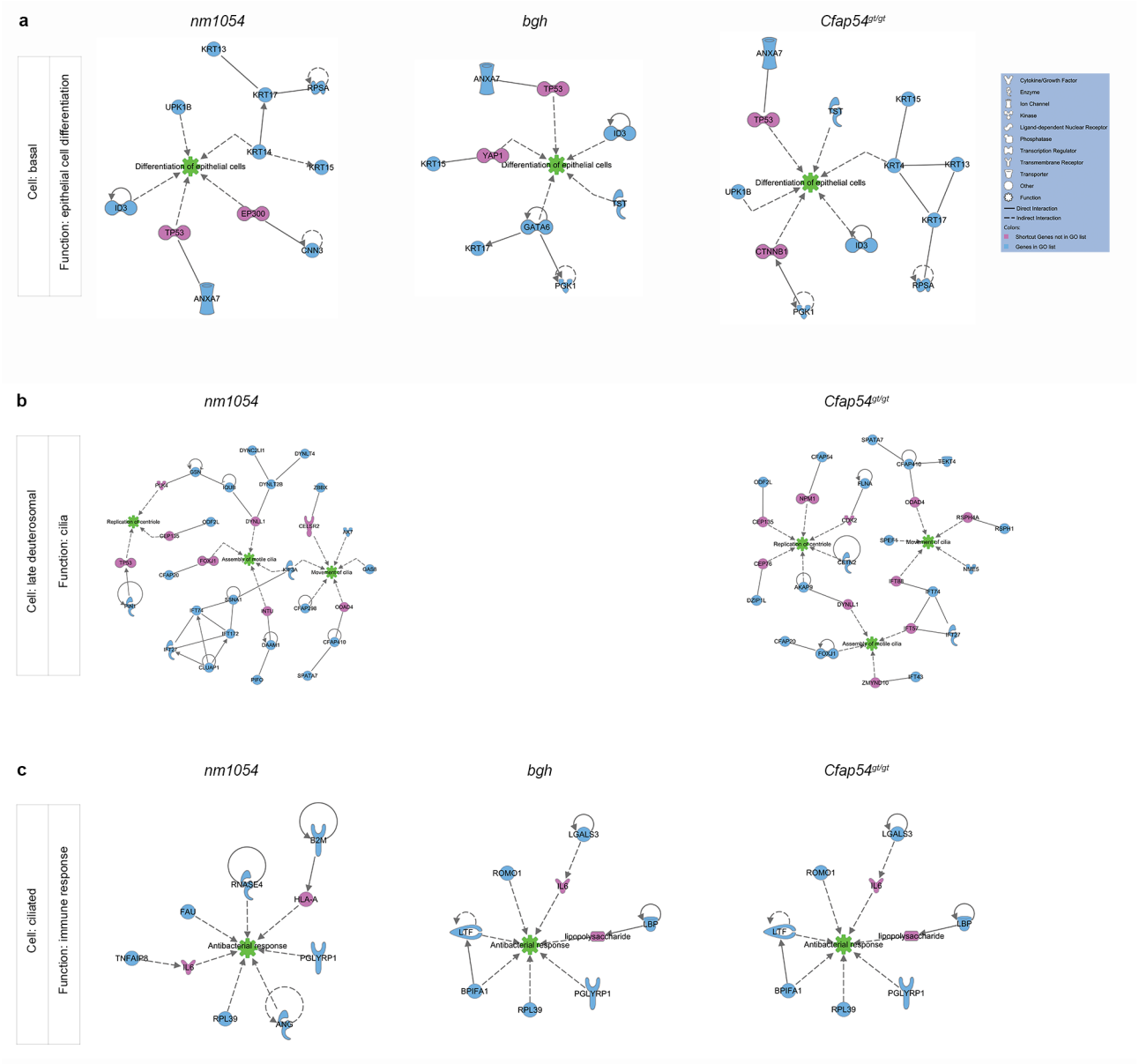

Fig. 6. Functional network diagrams for differentially expressed genes in *nm1054*, *bgh*, and *Cfap54*$^{gt/gt}$ cells. Networks are shown for biologically relevant functional categories of epithelial cell differentiation in basal cells (**A**), cilia in late deuterosomal cells (**B**), and immune response in ciliated cells (**C**). Networks were generated using the Ingenuity Pathway Analysis software based on GO functional categories. Cilia-related functional categories were not identified for *bgh* late deuterosomal cells through GO analysis.

The presence of an Unknown and unidentified cell cluster was both fascinating and unexpected. Analysis of marker genes confirmed that it is not one of the expected airway epithelial cell types or a common contaminant cell type such as fibroblasts, blood cells, macrophages, or lymphocytes (Fig. 2 and S2). We also confirmed that it does not express markers of intestinal epithelial cell types that might share a common origin or function with this cluster, much as the tuft cells or ionocytes do in both systems (Fig. S3). GO enrichment analysis identified the neuron-specific function of myelin sheath as a top function category for genes differentially expressed in this cluster relative to all other clusters in the sample (Fig. S4). It is possible that the Unknown cell type could have a nervous system origin, but further lineage studies are needed to definitively determine the identity of this cell cluster.

The presence of two distinct deuterosomal cell clusters in our analyses was also an unexpected finding. While both clusters express deuterosomal cell markers, they separate into individual clusters on the UMAP plot based on their gene expression profile (Fig. 2). GO enrichment analysis revealed that these clusters differ primarily in areas of microtubule cytoskeleton, cell projection, and ciliogenesis, suggesting that the early and late deuterosomal cells are at distinct stages in the differentiation path toward the ciliated cell type and represent distinct intermediate cell types. Affected pathways involved in cilium assembly, cell-cell contact, and Wnt

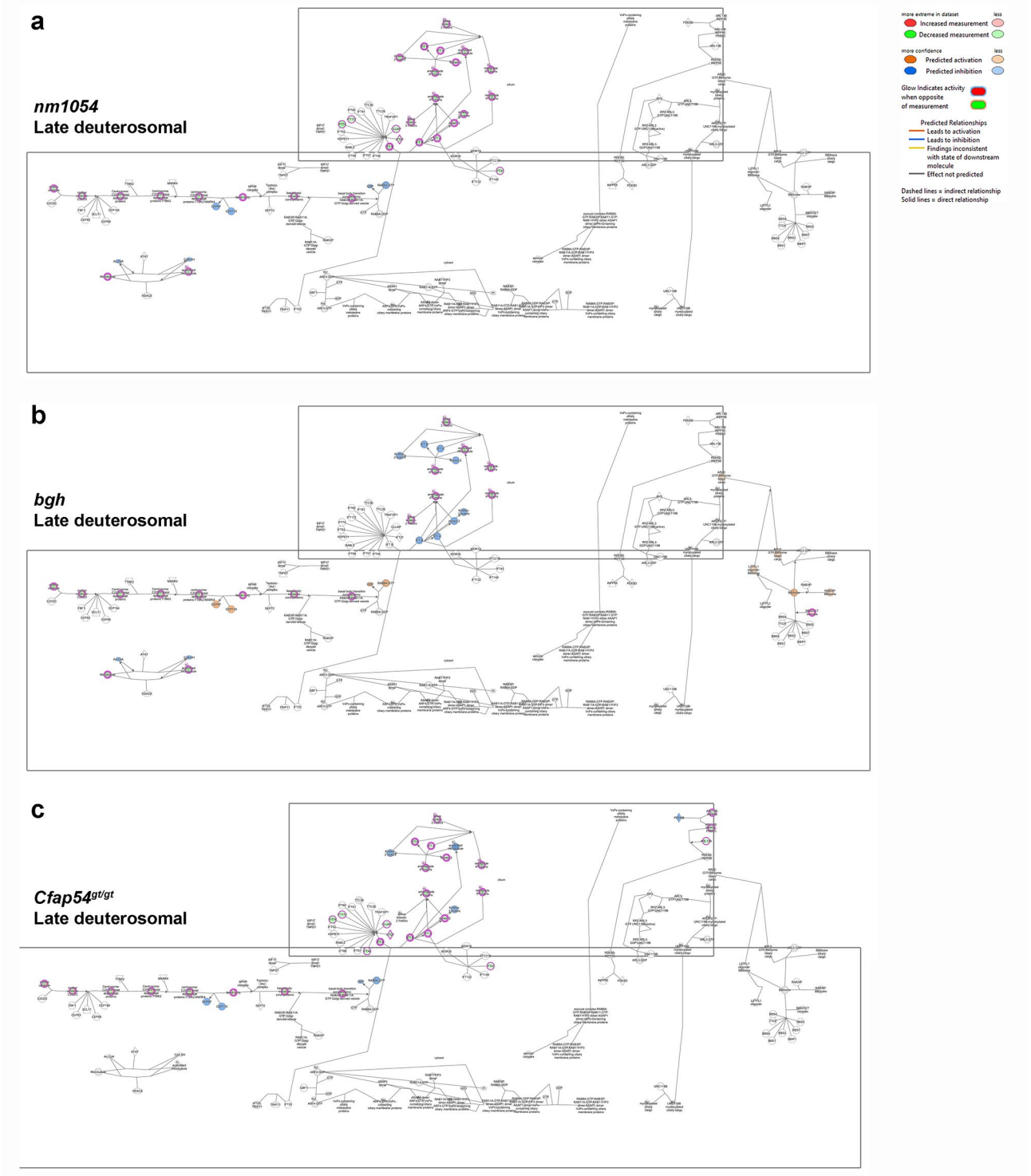

Fig. 7. Altered motile cilium assembly pathway in mutant deuterosomal cells. Pathway analysis shows differentially expressed genes involved in the cilium assembly pathway in *nm1054* (**A**), *bgh* (**B**), and *Cfap54*$^{gt/gt}$ (**C**) late deuterosomal cells. Pathway diagrams were generated using the Qiagen Ingenuity Pathway Analysis software.

signaling indicate that the late deuterosomal cells are undergoing important structural changes that may be driven by Wnt signaling. While additional lineage studies are required to more fully understand the nature and function of early and late deuterosomal cells, identification of these cells is an important and novel finding regarding the differentiation of epithelial cells in the airway.

The *nm1054*, *bgh*, and *Cfap54*$^{gt/gt}$ mice each have mutations in genes that encode components of the ciliary CPA (*Cfap221*, *Spef2*, and *Cfap54*, respectively), suggesting that they all contribute to the role of the CPA in regulating dynein motor force and ciliary beating[2]. Cfap221 and Cfap54 are also members of the same protein complex in *Chlamydomonas reinhardtii* flagella[30–32]. However, the DEGs and corresponding cellular functions affected in the early deuterosomal, late deuterosomal, and ciliated cells where the *Cfap221*, *Spef2*, and *Cfap54* genes are expressed are not identical across the three mutant mice. This is evident from distinct separation of the cell clusters by genotype on UMAP plots (Fig. 5) and differences in DEGs identified (Figs S8, S9, and S10; Table 1 and Tables S3-S8). Differences in DEGs also manifest in variations between mutants for functional gene networks and pathways (Figs. 6 and 7, S11, S12). This finding underscores the complexity of the CPA and demonstrates that mutations in specific genes may produce distinct phenotypes and cellular responses, even if their gene products are in the same protein complex.

DEG and functional enrichment analysis identified cellular functions of particular interest for differentiating ciliated cells in the PCD airway. Identification of cilia as a high priority functional category for late deuterosomal cells, which directly give rise to the ciliated cell type, suggests an alteration in epithelial cell differentiation (Fig. 6). Interestingly, cilia only emerged as a top functional category in GO enrichment analysis for the *nm1054* and *Cfap54*$^{gt/gt}$ late deuterosomal cells, suggesting that defects resulting from loss of Spef2 in the *bgh* mutant may not have the same impact on differentiation into the ciliated cell type as loss of Cfap221 or Cfap54. All three mutants, however, showed decreased expression of components of the cilium assembly pathway and a general down-regulation of that pathway (Fig. 7), indicating that differentiation of the ciliated cell type is inhibited in the mutant late deuterosomal cells. Several critical genes involved in intraflagellar transport (IFT), the cellular process underlying assembly of the cilium, are down-regulated in the *nm1054* and *Cfap54*$^{gt/gt}$ late deuterosomal cells, including *IFT27*, *IFT43*, *IFT74*, and *IFT172*. IFT27 is a critical component of the IFT machinery involved in both anterograde and retrograde transport during ciliogenesis[33]. Mutations in *IFT43* impair retrograde IFT transport in primary cilia and result in the human primary ciliopathy Sensenbrenner syndrome[34]. Mutations in *IFT74* result in human ciliopathies with defects in both primary and motile cilia, including the airway epithelial cilia[35,36]. *IFT172* mutations also affect formation of primary cilia and result in human ciliopathies Jeune syndrome and Mainzer-Saldino syndrome[37]. Similarly down-regulated in *nm1054* and *Cfap54*$^{gt/gt}$ late deuterosomal cells is *Dync2li1*, which encodes a light intermediate chain of the dynein 2 motor protein involved in transport of IFT particles during primary ciliogenesis and has been implicated in the human ciliopathy short rib polydactyly syndrome[38]. *Foxj1*, which is a critical transcription factor and regulator of the ciliary transcriptome and ciliated cell differentiation[39,40], is down-regulated in the *nm1054* and *bgh* late deuterosomal cells. Mutations in *FOXJ1* perturb ciliogenesis and result in a PCD phenotype in both humans and mice[41–43]. In addition, the gene encoding Cimap3, also known as pitchfork (Pifo), was down-regulated in all three mutant late deuterosomal cells. Cimap3 plays a role in sonic hedgehog (Shh) signaling and associates with assembling and disassembling primary cilia, with mutations resulting in human ciliopathies characterized by defects in ciliary dynamics[44,45]. Decreased expression of these genes further indicates that late deuterosomal cells exhibit a decrease in differentiation into ciliated cells.

Four additional PCD genes are down-regulated in the *nm1054* and *Cfap54*$^{gt/gt}$ late deuterosomal cells: *Ak7*, *Gas8*, *Rsph1*, and *Nme5*. *Ak7* has been implicated in both human PCD and a comparable mouse phenotype that includes mucus accumulation in the sinus cavity due to ciliary structural and motility defects[46,47]. *Nme5* mutations result in human PCD with associated respiratory infections, bronchiectasis, and ciliary structural defects[48], as well as a PCD phenotype with respiratory infections in Alaskan Malamute dogs[49]. Mutations in *Gas8*, which is down-regulated only in the *nm1054* late deuterosomal cells, result in human PCD with chronic respiratory infection and bronchiectasis due to ciliary structural defects[50], and mice lacking Gas8 have tracheal ciliary motility defects[51]. Human mutations in *RSPH1*, which is down-regulated only in *Cfap54*$^{gt/gt}$ late deuterosomal cells, result in PCD with associated chronic respiratory infections due to structural ciliary defects[52–54].

We identified immune response as a high-priority functional category for DEGs in ciliated cells (Fig. 6). Mucus clearance through ciliary beating is the primary function of ciliated cells in the airway. Analysis of DEGs in the ciliated cells would indicate how these cells are responding to a perturbation of their primary function. It stands to reason that the cells would respond by modifying immune function, which serves as the secondary means of defense after mucociliary clearance. Several genes of interest were found to be differentially regulated in the mutant ciliated cells. The gene encoding galectin-3 (*Lgals3*), which has been shown to promote neutrophil invasion via its own up-regulation during streptococcal pneumonia in mouse lungs[55,56], is also up-regulated in the *bgh* and *Cfap54*$^{gt/gt}$ ciliated cells. Similarly, up-regulated in the same mutants is the gene encoding the lipopolysaccharide (LPS)-binding protein (LBP), which has an inhibitory role in LPS-induced lung inflammation in mice[57]. *Bpifa1*, also known as *Splunc1*, is down-regulated in *bgh* and *Cfap54*$^{gt/gt}$ ciliated cells. Mouse studies have shown that Bpifa1 promotes the lung innate immune response upon bacterial infection[58–60]. The gene encoding TNF-α-induced protein 8 (*Tnfaip8*) is down-regulated in *nm1054* and *Cfap54*$^{gt/gt}$ ciliated cells and has been shown to regulate bacterial invasion in the liver, spleen, and intestine[61,62], although its role in airway immune response is unknown. Inhibition or loss of Pglyrp1 in mice results in increased susceptibility to infection and impaired inflammatory response in the airway[63,64]. The *Pglyrp1* gene is differentially expressed in ciliated cells from all three mutants, but it is up-regulated in the *bgh* mutant and down-regulated in *nm1054* and *Cfap54*$^{gt/gt}$ ciliated cells. While the mechanisms of altered immune response in mutant ciliated cells remains to be determined, it is clear that expression of related genes is affected, and the response may vary depending on the specific mutation and ciliary defect. Taken together, the DEG analyses in this study shed light on cellular responses to ciliary dysfunction in the airway and enhance the current understanding of the ciliary microenvironment.

Materials and methods

Mice The *Mus musculus nm1054* line lacking *Cfap221*, the *bgh* line with a mutation in *Spef2*, and the *Cfap54*$^{gt/gt}$ line with a gene-trapped allele of *Cfap54* were obtained as previously described[20–22], and each line was maintained on the 129S6/SvEvTac (129) background. Mice heterozygous for these lines and wild type controls were bred to B6;C3-Tg(FOXJ1-EGFP)85Leo/J mice (Jackson Laboratory, strain 010827) expressing *EGFP* under the *Foxj1* promoter[65], providing EGFP as a positive control marker for ciliated and deuterosomal cells. Mice that were homozygous for the *Cfap221*, *Cfap54*, and *Spef2* mutations and expressed EGFP under the *Foxj1* promoter were used for single-cell RNA sequencing experiments. Other than male infertility, no sex-specific differences have been observed for the PCD phenotypes associated with the *nm1054*, *bgh*, or *Cfap54gt/gt* lines[20–22]. Therefore, male and female mice were used for pooled samples in this study. All experiments involving mice were performed in accordance with the Animal Welfare Act and National Institutes of Health (NIH) policies and were approved by the Sanford Research Institutional Animal Care and Use Committee under protocol 2023-0087. Per AVMA guidelines, mice were euthanized by inhalation of carbon dioxide without anesthesia followed by cervical dislocation. The carbon dioxide is delivered from a compressed tank to the cage at a flow rate of 30% cage volume displacement. This is monitored and verified by our attending veterinarian, and it complies with the ARRIVE guidelines.

Tracheal epithelial cell preparation Five to six mice were pooled from each genotype for scRNAseq sample preparation (6 WT, 6 *nm1054*, 5 *bgh*, 6 *Cfap54*$^{gt/gt}$). Each mouse was between five and eight months of age at the time of sample collection. Because no age-specific differences have been observed in the airway pathology of any of these lines, and tissue damage has not been observed as a result of mucus accumulation, there were no concerns about precise age matching[20–23,29]. Tracheae were removed from the mice, and the cells were isolated as described by You and Brody, 2013 [66]. In brief, cells were dissociated in Pronase solution (1.5 mg/ml, Roche, #11-459-643-001) and plated on Primaria cell culture dishes for three to four hours to separate the epithelial cells from the fibroblasts. Dead cells were removed from the epithelial suspension using the Miltenyi Biotec Dead Cell Cleanup Kit (#130-090-101), and the cells were passed through a 40-micron Flowmi Cell Strainer (SP Bel-Art Scienceware) before collecting the live cells using a MiniMACS Separator column (Miltenyi Biotec). For each genotype, cells were resuspended in Hams F-12 media with 10% fetal bovine serum to a final count of 1×10^6 cells/ml.

Single cell RNA sequencing For each genotype, 8500 cells were loaded into Chromium Next GEM Chip G (10X Genomics, #1000120) in the reverse transcription reaction according to the manufacturer's instructions to capture at least 5000 cells. Reverse transcription, gel beads-in-emulsion (GEM) generation, and library preparation were performed using the Chromium Next GEM Single Cell 3' Kit v3.1 (10X Genomics, #1000268). Gel beads were loaded into the designated wells of the same Chip G, which was then inserted into the Chromium Controller for GEM generation. Following GEM generation, full-length barcoded cDNAs were produced from poly-adenylated mRNA by reverse transcription, and the cDNA was amplified using twelve amplification cycles per manufacturer recommendation. The amplified cDNA was cleaned up using SPRIselect (Beckman Coulter), and the cDNA (1 µl) was run on a bioanalyzer using the High Sensitivity DNA kit (Agilent, #5067 − 4627) to assess the quality and determine concentration. To prepare Illumina sequencing-compatible cDNA libraries, the cDNA was subjected to fragmentation, followed by end repair, A-tailing, and adapter ligation. After each of these steps, the reaction product was cleaned up using SPRIselect. The samples were then amplified with dual sample indexes to enable multiplexing during sequencing, cleaned up, and quantified. The cDNA (0.5 ng/ml) was sequenced by Novogene.

Bioinformatics scRNA-seq reads were aligned using CellRanger (10X Genomics, version 6.0.1) with default parameters[67]. Initially, a CellRanger count was performed on each sample, followed by CellRanger aggregation to generate a consolidated expression matrix, a vector of genes, and a vector of barcodes. The resulting expression matrix, along with the gene and barcode vectors, was imported into R Studio (version 4.3.1) for further analysis using the Seurat package (version 4.0.4)[68,69]. Seurat was employed for the single cell analysis, including differential expression analysis. Default settings to produce DEG lists based on the non-parametric Wilcoxon rank sum test included a Log(fold change) threshold of 0.1 and a min.pct fraction of 0.01. Prior to clustering, cells underwent filtering based on the percentage of mitochondrial RNA (< 10%) and the number of genes expressed, with cell cycle correction applied. Cluster identification and pseudotime trajectory analysis were facilitated by Monocle3 (version 1.2.9)[69–72] and Slingshot (version 2.12.0)[73]. Garnett (version 0.2.8) and its mmLung pretrained classifier were utilized for cell type classification in the single-cell expression data[74]. Cluster boundaries were defined using Loupe Browser (10X Genomics) to identify regions of cell-specific marker expression. Gene ontology classification of differentially expressed genes was performed using DAVID[75,76], and network and pathway analyses were performed using the Ingenuity Pathway Analysis software (Qiagen)[77].

Data availability

The single cell RNAseq datasets generated and analyzed in this study are available in the NCBI Gene Expression Omnibus (GEO) database under accession number GSE254100. Prior to release, they are available to reviewers at the following link by entering the token "ongvmmagtxcrnox": https://www.ncbi.nlm.nih.gov/geo/query/acc.cgi? acc=GSE254100.

Received: 20 September 2024; Accepted: 13 November 2024
Published online: 18 November 2024

References

1. Wallmeier, J. et al. Motile ciliopathies. *Nat. Rev. Dis. Primers.* **6**, 77. https://doi.org/10.1038/s41572-020-0209-6 (2020).
2. Lee, L. & Ostrowski, L. E. Motile cilia genetics and cell biology: big results from little mice. *Cell. Mol. Life Sci.* **78**, 769–797. https://doi.org/10.1007/s00018-020-03633-5 (2021).
3. Shoemark, A. & Harman, K. Primary ciliary Dyskinesia. *Semin Respir Crit. Care Med.* **42**, 537–548. https://doi.org/10.1055/s-0041-1730919 (2021).
4. Zaragosi, L. E., Deprez, M. & Barbry, P. Using single-cell RNA sequencing to unravel cell lineage relationships in the respiratory tract. *Biochem. Soc. Trans.* **48**, 327–336. https://doi.org/10.1042/BST20191010 (2020).
5. Montoro, D. T. et al. A revised airway epithelial hierarchy includes CFTR-expressing ionocytes. *Nature.* **560**, 319–324. https://doi.org/10.1038/s41586-018-0393-7 (2018).
6. Plasschaert, L. W. et al. A single-cell atlas of the airway epithelium reveals the CFTR-rich pulmonary ionocyte. *Nature.* **560**, 377–381. https://doi.org/10.1038/s41586-018-0394-6 (2018).
7. Ruiz Garcia, S. et al. Novel dynamics of human mucociliary differentiation revealed by single-cell RNA sequencing of nasal epithelial cultures. *Development*. **146** https://doi.org/10.1242/dev.177428 (2019).
8. Deprez, M. et al. A single-cell atlas of the Human Healthy Airways. *Am. J. Respir Crit. Care Med.* **202**, 1636–1645. https://doi.org/10.1164/rccm.201911-2199OC (2020).
9. Travaglini, K. J. et al. A molecular cell atlas of the human lung from single-cell RNA sequencing. *Nature*. **587**, 619–625. https://doi.org/10.1038/s41586-020-2922-4 (2020).
10. Wijk, S. C. et al. Human primary airway basal cells display a Continuum of Molecular Phases from Health to Disease in Chronic Obstructive Pulmonary Disease. *Am. J. Respir Cell. Mol. Biol.* **65**, 103–113. https://doi.org/10.1165/rcmb.2020-0464OC (2021).
11. Kadur, L. et al. Human distal lung maps and lineage hierarchies reveal a bipotent progenitor. *Nature*. **604**, 111–119. https://doi.org/10.1038/s41586-022-04541-3 (2022).
12. Paranjapye, A., Leir, S. H., Huang, F., Kerschner, J. L. & Harris, A. Cell function and identity revealed by comparative scRNA-seq analysis in human nasal, bronchial and epididymis epithelia. *Eur. J. Cell. Biol.* **101**, 151231. https://doi.org/10.1016/j.ejcb.2022.151231 (2022).
13. Miller, A. J. et al. In Vitro and in vivo development of the human airway at single-cell resolution. *Dev. Cell.* **54**, 818. https://doi.org/10.1016/j.devcel.2020.09.012 (2020).
14. Cao, S. et al. Single-cell RNA sequencing reveals the developmental program underlying proximal-distal patterning of the human lung at the embryonic stage. *Cell. Res.* **33**, 421–433. https://doi.org/10.1038/s41422-023-00802-6 (2023).
15. Chae, S., Park, T. J. & Kwon, T. Convergent differentiation of multiciliated cells. *Sci. Rep.* **13**, 23028. https://doi.org/10.1038/s41598-023-50077-5 (2023).
16. Reyfman, P. A. et al. Single-cell transcriptomic analysis of human lung provides insights into the Pathobiology of Pulmonary Fibrosis. *Am. J. Respir Crit. Care Med.* **199**, 1517–1536. https://doi.org/10.1164/rccm.201712-2410OC (2019).
17. Carraro, G. et al. Transcriptional analysis of cystic fibrosis airways at single-cell resolution reveals altered epithelial cell states and composition. *Nat. Med.* **27**, 806–814. https://doi.org/10.1038/s41591-021-01332-7 (2021).
18. Yang, W. et al. Multiomics Analysis of a DNAH5-Mutated PCD Organoid Model revealed the key role of the TGF-beta/BMP and notch pathways in epithelial differentiation and the Immune response in DNAH5-Mutated patients. *Cells*. **11**, 4013. https://doi.org/10.3390/cells11244013 (2022).
19. Horani, A. et al. The effect of Dnaaf5 gene dosage on primary ciliary dyskinesia phenotypes. *JCI Insight*. **8**, e168836. https://doi.org/10.1172/jci.insight.168836 (2023).
20. Lee, L. et al. Primary ciliary dyskinesia in mice lacking the novel ciliary protein Pcdp1. *Mol. Cell. Biol.* **28**, 949–957. https://doi.org/10.1128/MCB.00354-07 (2008).
21. Sironen, A. et al. Loss of SPEF2 function in mice results in spermatogenesis defects and primary ciliary Dyskinesia. *Biol. Reprod.* **85**, 690–701. https://doi.org/10.1095/biolreprod.111.091132 (2011). doi:biolreprod.111.091132 [pii].
22. McKenzie, C. W. et al. CFAP54 is required for proper ciliary motility and assembly of the central pair apparatus in mice. *Mol. Biol. Cell.* **26**, 3140–3149. https://doi.org/10.1091/mbc.E15-02-0121 (2015).
23. McKenzie, C. W. et al. Enhanced response to pulmonary Streptococcus pneumoniae infection is associated with primary ciliary dyskinesia in mice lacking Pcdp1 and Spef2. *Cilia* 2, 18, doi: (2013). https://doi.org/10.1186/2046-2530-2-18
24. Bustamante-Marin, X. M. et al. Identification of genetic variants in CFAP221 as a cause of primary ciliary dyskinesia. *J. Hum. Genet.* **65**, 175–180. https://doi.org/10.1038/s10038-019-0686-1 (2020).
25. Cindric, S. et al. SPEF2- and HYDIN-Mutant cilia lack the Central Pair-associated protein SPEF2, aiding primary ciliary Dyskinesia Diagnostics. *Am. J. Respir Cell. Mol. Biol.* **62**, 382–396. https://doi.org/10.1165/rcmb.2019-0086OC (2020).
26. Zhao, X. et al. Lack of CFAP54 causes primary ciliary dyskinesia in a mouse model and human patients. *Front. Med.* https://doi.org/10.1007/s11684-023-0997-7 (2023).
27. Cooney, R. A. et al. A WNT4- and DKK3-driven canonical to noncanonical wnt signaling switch controls multiciliogenesis. *J. Cell. Sci.* **136** https://doi.org/10.1242/jcs.260807 (2023).
28. Seidl, C. et al. Mucociliary wnt signaling promotes cilia biogenesis and beating. *Nat. Commun.* **14**, 1259. https://doi.org/10.1038/s41467-023-36743-2 (2023).
29. McKenzie, C. W. & Lee, L. Genetic interaction between central pair apparatus genes CFAP221, CFAP54, and SPEF2 in mouse models of primary ciliary dyskinesia. *Sci. Rep.* **10**, 12337. https://doi.org/10.1038/s41598-020-69359-3 (2020).
30. Brown, J. M., Dipetrillo, C. G., Smith, E. F. & Witman, G. B. A FAP46 mutant provides new insights into the function and assembly of the C1d complex of the ciliary central apparatus. *J Cell Sci* 125, 3904–3913, doi:jcs.107151 [pii] (2012). https://doi.org/10.1242/jcs.107151
31. DiPetrillo, C. G. & Smith, E. F. Pcdp1 is a central apparatus protein that binds Ca(2+)-calmodulin and regulates ciliary motility. *J Cell Biol* 189, 601–612, doi:jcb.200912009 [pii] (2010). https://doi.org/10.1083/jcb.200912009
32. DiPetrillo, C. G. & Smith, E. F. The Pcdp1 complex coordinates the activity of dynein isoforms to produce wild-type ciliary motility. *Mol. Biol. Cell.* **22**, 4527–4538. https://doi.org/10.1091/mbc.E11-08-0739 (2011). doi:mbc.E11-08-0739 [pii].
33. Huet, D., Blisnick, T., Perrot, S. & Bastin, P. The GTPase IFT27 is involved in both anterograde and retrograde intraflagellar transport. *Elife*. **3**, e02419. https://doi.org/10.7554/eLife.02419 (2014).
34. Arts, H. H. et al. C14ORF179 encoding IFT43 is mutated in Sensenbrenner syndrome. *J. Med. Genet.* **48**, 390–395. https://doi.org/10.1136/jmg.2011.088864 (2011).
35. Bakey, Z. et al. IFT74 variants cause skeletal ciliopathy and motile cilia defects in mice and humans. *PLoS Genet.* **19**, e1010796. https://doi.org/10.1371/journal.pgen.1010796 (2023).
36. Fassad, M. R. et al. Defective airway intraflagellar transport underlies a combined motile and primary ciliopathy syndrome caused by IFT74 mutations. *Hum. Mol. Genet.* **32**, 3090–3104. https://doi.org/10.1093/hmg/ddad132 (2023).
37. Halbritter, J. et al. Defects in the IFT-B component IFT172 cause Jeune and Mainzer-Saldino syndromes in humans. *Am. J. Hum. Genet.* **93**, 915–925. https://doi.org/10.1016/j.ajhg.2013.09.012 (2013).
38. Taylor, S. P. et al. Mutations in DYNC2LI1 disrupt cilia function and cause short rib polydactyly syndrome. *Nat. Commun.* **6**, 7092. https://doi.org/10.1038/ncomms8092 (2015).
39. Mukherjee, I., Roy, S. & Chakrabarti, S. Identification of important effector proteins in the FOXJ1 Transcriptional Network Associated with ciliogenesis and ciliary function. *Front. Genet.* **10**, 23. https://doi.org/10.3389/fgene.2019.00023 (2019).

40. You, Y. et al. Role of f-box factor foxj1 in differentiation of ciliated airway epithelial cells. *Am. J. Physiol. Lung Cell. Mol. Physiol.* **286**, L650–657. https://doi.org/10.1152/ajplung.00170.2003 (2004).
41. Chen, J., Knowles, H. J., Hebert, J. L. & Hackett, B. P. Mutation of the mouse hepatocyte nuclear factor/forkhead homologue 4 gene results in an absence of cilia and random left-right asymmetry. *J. Clin. Invest.* **102**, 1077–1082 (1998).
42. Brody, S. L., Yan, X. H., Wuerffel, M. K., Song, S. K. & Shapiro, S. D. Ciliogenesis and left-right axis defects in forkhead factor HFH-4-null mice. *Am. J. Respir Cell. Mol. Biol.* **23**, 45–51 (2000).
43. Wallmeier, J. et al. De Novo mutations in FOXJ1 result in a motile ciliopathy with Hydrocephalus and Randomization of Left/Right body asymmetry. *Am. J. Hum. Genet.* **105**, 1030–1039. https://doi.org/10.1016/j.ajhg.2019.09.022 (2019).
44. Kinzel, D. et al. Pitchfork regulates primary cilia disassembly and left-right asymmetry. *Dev. Cell.* **19**, 66–77. https://doi.org/10.1016/j.devcel.2010.06.005 (2010).
45. Jung, B. et al. Pitchfork and Gprasp2 Target smoothened to the primary cilium for hedgehog pathway activation. *PLoS One.* **11**, e0149477. https://doi.org/10.1371/journal.pone.0149477 (2016).
46. Fernandez-Gonzalez, A., Kourembanas, S., Wyatt, T. A. & Mitsialis, S. A. Mutation of murine adenylate kinase 7 underlies a primary ciliary dyskinesia phenotype. *Am. J. Respir Cell. Mol. Biol.* **40**, 305–313 (2009).
47. Mata, M. et al. New adenylate kinase 7 (AK7) mutation in primary ciliary dyskinesia. *Am. J. Rhinol Allergy*. **26**, 260–264. https://doi.org/10.2500/ajra.2012.26.3784 (2012).
48. Cho, E. H. et al. A nonsense variant in NME5 causes human primary ciliary dyskinesia with radial spoke defects. *Clin. Genet.* **98**, 64–68. https://doi.org/10.1111/cge.13742 (2020).
49. Anderegg, L. et al. NME5 frameshift variant in alaskan malamutes with primary ciliary dyskinesia. *PLoS Genet.* **15**, e1008378. https://doi.org/10.1371/journal.pgen.1008378 (2019).
50. Olbrich, H. et al. Loss-of-function GAS8 mutations cause primary ciliary Dyskinesia and disrupt the Nexin-Dynein Regulatory Complex. *Am. J. Hum. Genet.* **97**, 546–554. https://doi.org/10.1016/j.ajhg.2015.08.012 (2015).
51. Lewis, W. R. et al. Mutation of growth arrest specific 8 reveals a role in motile cilia function and human disease. *PLoS Genet.* **12**, e1006220. https://doi.org/10.1371/journal.pgen.1006220 (2016).
52. Kott, E. et al. Loss-of-function mutations in RSPH1 cause primary ciliary dyskinesia with central-complex and radial-spoke defects. *Am. J. Hum. Genet.* **93**, 561–570. https://doi.org/10.1016/j.ajhg.2013.07.013 (2013).
53. Onoufriadis, A. et al. Targeted NGS gene panel identifies mutations in RSPH1 causing primary ciliary dyskinesia and a common mechanism for ciliary central pair agenesis due to radial spoke defects. *Hum. Mol. Genet.* **23**, 3362–3374. https://doi.org/10.1093/hmg/ddu046 (2014).
54. Knowles, M. R. et al. Mutations in RSPH1 cause primary ciliary dyskinesia with a unique clinical and ciliary phenotype. *Am. J. Respir Crit. Care Med.* **189**, 707–717. https://doi.org/10.1164/rccm.201311-2047OC (2014).
55. Sato, S. et al. Role of galectin-3 as an adhesion molecule for neutrophil extravasation during streptococcal pneumonia. *J. Immunol.* **168**, 1813–1822. https://doi.org/10.4049/jimmunol.168.4.1813 (2002).
56. Nieminen, J., St-Pierre, C., Bhaumik, P., Poirier, F. & Sato, S. Role of galectin-3 in leukocyte recruitment in a murine model of lung infection by Streptococcus pneumoniae. *J. Immunol.* **180**, 2466–2473. https://doi.org/10.4049/jimmunol.180.4.2466 (2008).
57. Knapp, S., Florquin, S., Golenbock, D. T. & van der Poll, T. Pulmonary lipopolysaccharide (LPS)-binding protein inhibits the LPS-induced lung inflammation in vivo. *J. Immunol.* **176**, 3189–3195. https://doi.org/10.4049/jimmunol.176.5.3189 (2006).
58. Gally, F. et al. SPLUNC1 promotes lung innate defense against Mycoplasma pneumoniae infection in mice. *Am. J. Pathol.* **178**, 2159–2167. https://doi.org/10.1016/j.ajpath.2011.01.026 (2011).
59. Lukinskiene, L. et al. Antimicrobial activity of PLUNC protects against Pseudomonas aeruginosa infection. *J. Immunol.* **187**, 382–390. https://doi.org/10.4049/jimmunol.1001769 (2011).
60. Liu, Y. et al. Increased susceptibility to pulmonary Pseudomonas infection in Splunc1 knockout mice. *J. Immunol.* **191**, 4259–4268. https://doi.org/10.4049/jimmunol.1202340 (2013).
61. Porturas, T. P. et al. Crucial roles of TNFAIP8 protein in regulating apoptosis and Listeria infection. *J. Immunol.* **194**, 5743–5750. https://doi.org/10.4049/jimmunol.1401987 (2015).
62. Sun, H. et al. Exacerbated experimental colitis in TNFAIP8-deficient mice. *J. Immunol.* **194**, 5736–5742. https://doi.org/10.4049/jimmunol.1401986 (2015).
63. Osanai, A. et al. Mouse peptidoglycan recognition protein PGLYRP-1 plays a role in the host innate immune response against Listeria monocytogenes infection. *Infect. Immun.* **79**, 858–866. https://doi.org/10.1128/IAI.00466-10 (2011).
64. Yao, X. et al. Peptidoglycan recognition protein 1 promotes house dust mite-induced airway inflammation in mice. *Am. J. Respir Cell. Mol. Biol.* **49**, 902–911. https://doi.org/10.1165/rcmb.2013-0001OC (2013).
65. Ostrowski, L. E., Hutchins, J. R., Zakel, K. & O'Neal, W. K. Targeting expression of a transgene to the airway surface epithelium using a ciliated cell-specific promoter. *Mol. Ther.* **8**, 637–645. https://doi.org/10.1016/s1525-0016(03)00221-1 (2003).
66. You, Y. & Brody, S. L. Culture and differentiation of mouse tracheal epithelial cells. *Methods Mol. Biol.* **945**, 123–143. https://doi.org/10.1007/978-1-62703-125-7_9 (2013).
67. Zheng, G. X. et al. Massively parallel digital transcriptional profiling of single cells. *Nat. Commun.* **8**, 14049. https://doi.org/10.1038/ncomms14049 (2017).
68. Hao, Y. et al. Integrated analysis of multimodal single-cell data. *Cell* 184, 3573–3587 e3529, doi: (2021). https://doi.org/10.1016/j.cell.2021.04.048
69. Cao, J. et al. The single-cell transcriptional landscape of mammalian organogenesis. *Nature*. **566**, 496–502. https://doi.org/10.1038/s41586-019-0969-x (2019).
70. Trapnell, C. et al. The dynamics and regulators of cell fate decisions are revealed by pseudotemporal ordering of single cells. *Nat. Biotechnol.* **32**, 381–386. https://doi.org/10.1038/nbt.2859 (2014).
71. Qiu, X. et al. Reversed graph embedding resolves complex single-cell trajectories. *Nat. Methods*. **14**, 979–982. https://doi.org/10.1038/nmeth.4402 (2017).
72. Becht, E. et al. Dimensionality reduction for visualizing single-cell data using UMAP. *Nat. Biotechnol.* **37**, 38–44. https://doi.org/10.1038/nbt.4314 (2018).
73. Street, K. et al. Slingshot: cell lineage and pseudotime inference for single-cell transcriptomics. *BMC Genom.* **19**, 477. https://doi.org/10.1186/s12864-018-4772-0 (2018).
74. Pliner, H. A., Shendure, J. & Trapnell, C. Supervised classification enables rapid annotation of cell atlases. *Nat. Methods*. **16**, 983–986. https://doi.org/10.1038/s41592-019-0535-3 (2019).
75. Sherman, B. T. et al. DAVID: a web server for functional enrichment analysis and functional annotation of gene lists (2021 update). *Nucleic Acids Res.* **50**, W216–W221. https://doi.org/10.1093/nar/gkac194 (2022).
76. Huang da, W., Sherman, B. T. & Lempicki, R. A. Systematic and integrative analysis of large gene lists using DAVID bioinformatics resources. *Nat. Protoc.* **4**, 44–57. https://doi.org/10.1038/nprot.2008.211 (2009).
77. Kramer, A., Green, J., Pollard, J. Jr. & Tugendreich, S. Causal analysis approaches in Ingenuity Pathway Analysis. *Bioinformatics*. **30**, 523–530. https://doi.org/10.1093/bioinformatics/btt703 (2014).

Acknowledgements

We gratefully thank Malini Mukherjee for assistance with scRNAseq experiments and Yohannes Tecleab for assistance with bioinformatics analysis. This study was funded by Sanford Research and a Genetics and Genomics

grant from the Sanford Health Foundation. The Sanford Research Functional Genomics & Bioinformatics Core was supported by NIH CoBRE grant P20GM103620. R.M.W. was supported by NSF REU grant 1756912.

Author contributions

C.W.M. bred the mouse lines, performed the experiments, and analyzed the data. R.M.W., O.J.I., and M.S.K. analyzed the data. L.L. designed the study, analyzed the data, and wrote the manuscript. All authors read and approved the final manuscript.

Declarations

Competing interests

The authors declare no competing interests.

Additional information

Supplementary Information The online version contains supplementary material available at https://doi.org/10.1038/s41598-024-79877-z.

Correspondence and requests for materials should be addressed to L.L.

Reprints and permissions information is available at www.nature.com/reprints.

Publisher's note Springer Nature remains neutral with regard to jurisdictional claims in published maps and institutional affiliations.